metadata, citation and similar papers at core.ac.uk

brought to you by

provided by C

Estimating Species Abundance in a Northern Temperate Forest Using Spectral Mixture Analysis

Lucie C. Plourde, Scott V. Ollinger, Marie-Louise Smith, and Mary E. Martin

Abstract

Effective, reliable methods for characterizing the spatial distribution of tree species through remote sensing would represent an important step toward better understanding changes in biodiversity, habitat quality, climate, and nutrient cycling. Towards this end, we explore the feasibility of using spectral mixture analysis to discriminate the distribution and abundance of two important forest species at the Bartlett Experimental Forest, New Hampshire. Using hyperspectral image data and simulated broadband sensor data, we used spectral unmixing to quantify the abundance *of sugar maple and American beech, as opposed to the more conventional approach of detecting presence or absence of discrete species classes. Stronger linear relationships were demonstrated between predicted and measured abundance for hyperspectral than broadband sensor data: R^2 = 0.49 (RMSE = 0.09) versus R^2 = 0.16 (RMSE = 0.19) for sugar maple; R^2 = 0.36 (RMSE = 0.18) versus R^2 = 0.24 (RMSE = 0.33) for beech. These results suggest that spectrally unmixing hyperspectral data to estimate species abundances holds promise for a variety of ecological studies.*

Introduction

Characterizing the spatial distribution of tree species in forest ecosystems is central to a wide range of scientific and land management issues. Tree species mapping has long been of interest to managers concerned with biodiversity and habitat quality (e.g., Leak, 1982; Gansner *et al.*, 1996; Spetich *et al.*, 1997; Puttock *et al.*, 1998; Chokkalingam and White, 2001), and some of our most pressing present-day environmental concerns stem from the loss of native species, the spread of exotics, or shifts in distribution brought about by climate change (Allison and Vitousek, 2004; Iverson *et al.*, 1997; Drohan *et al.*, 2002).

Tree species identification has also become important in the study of biogeochemistry, where there is increasing interest in the role played by individual tree species as mediators of element cycles. For example, a number of studies have identified relationships between the abundance of sugar maple and soil properties associated with nitrogen cycling, such as soil carbon to nitrogen ratios and rates of nitrate export to aquatic ecosystems (e.g., Finzi *et al.*, 1998; Lovett *et al.*, 2004). As a consequence, concern over changes in sugar maple health and spatial patterning (caused either by stress-induced declines in growth (Horsley *et al.*, 2000; Bailey *et al.*, 2004) or by recent changes in competition with American beech (e.g., Hane, 2003)) also carries implications for alterations to the N cycle.

Given the importance of species-specific ecological interactions and potential consequences of changes in species distributions, reliable methods for remote sensing of forest composition at the species level would be a significant advancement towards understanding these dynamics. Although a number of studies have made important progress on this general topic (e.g., Woodcock *et al.*, 1994; Gilabert *et al.*, 2000; Leckie *et al.*, 2003), substantial challenges remain and standardized methods for creating species-level maps that are both spatially extensive and temporally dynamic are not well developed. Methods involving multispectral remote sensing instruments have proven useful for generating broadly-classified forest cover type maps (e.g., Schriever and Congalton, 1995; Watson and Wilcock, 2001), but have not proven robust in providing more detailed, species-level information. Given the additional spectral detail provided by imaging spectrometers, hyperspectral remote sensing has emerged as a potentially useful approach for distinguishing composition at the species level (e.g., Gong *et al.*, 1997; Kokaly *et al.*, 2003; Martin *et al.*, 1998; Roberts *et al.*, 1998; Ustin and Xiao, 2001). However, the number of investigations in heterogeneous temperate forests remains small and, of those that have been conducted, most have focused on other regions with relatively low species diversity and physiognomic composition.

Shifts in the abundance of sugar maple and American beech across the northeastern U.S. have been brought about by a combination of the spread of beech bark disease (Houston, 1994; Hane, 2003) beginning in the early 1950s and, in some regions, stress-induced decline of sugar maple (Horsley *et al.*, 2000; Bailey *et al.*, 2004). Given the importance of these species to the region and recent evidence of their differential effects on nutrient cycles (e.g., Lovett and Rueth, 1999), we sought to explore the degree to which we could estimate the abundance of these two species using spectral mixture

Lucie C. Plourde, Scott V. Ollinger, and Mary E. Martin are with the Complex Systems Research Center, Institute for the Study of Earth, Oceans, and Space, University of New Hampshire, Durham, NH 03824 (lucie.plourde@unh.edu).

Marie-Louise Smith is with the USDA Forest Service, Northern Research Station, 271 Mast Road, Durham, NH 03824.

Photogrammetric Engineering & Remote Sensing
Vol. 73, No. 7, July 2007, pp. 829–840.

0099-1112/07/7307–0829/$3.00/0
© 2007 American Society for Photogrammetry and Remote Sensing

analysis (e.g., Asner, *et al.*, 2003; Radeloff *et al.*, 1999; Gong *et al.*, 1994). Our main objective was to explore how well we could quantify the abundance of sugar maple and American beech across a diverse northeastern U.S. forest landscape by spectrally unmixing both airborne and space-borne hyperspectral imagery. Because hyperspectral data are not as widely available as broadband data, a secondary objective was to compare these results with a spectral mixture analysis of the hyperspectral imagery resampled to a multispectral sensor resolution. Finally, the ability to quantify species abundances would represent a significant improvement over the more conventional approach of mapping presence or absence of discrete forest types. To evaluate the degree of improvement gained, we also performed a supervised classification to enable comparison with spectral mixture analysis results.

Methods

Background

In the Northeastern United States, forests are characterized by heterogeneous species mixtures and age classes with landscape-level variation caused by factors such as topography, soils, and disturbance history. Because of their inherent spatial and temporal variability, northern temperate forests can be difficult to classify, even to a generalized "type" level. Moreover, labeling discrete forest type classes is often not the most meaningful classification approach. For many applications, measures of species' relative abundances across the landscape would provide a more useful representation of ground conditions.

A variety of optical remote sensing approaches have been used to create species classifications, including maximum likelihood classifiers, ISODATA techniques, spectral angle mapping, and spectral unmixing, or spectral mixture analysis (SMA). Among these, perhaps the most promising method for ascertaining species abundance is SMA, which allows separation of "background" material (e.g., shadows, areas of nonvegetation, tree species other than those of interest) from the material or species of interest (Roberts *et al.*, 1998; Ustin and Xiao, 2001; Dennison and Roberts, 2003). By "unmixing" pixels, abundances of user-defined endmembers can be identified.

One of the first steps in forest classification, then, typically involves developing a spectral library or identifying "endmembers," i.e., spectral signatures unique to a certain species or forest type (Williams and Hunt, 2002; Elmore *et al.*, 2000; Alberotanza *et al.*, 1999; Sandmeier and Deering, 1999; Roberts *et al.*, 1998; Sohn and McCoy, 1997; García-Haro *et al.*, 1996). In multispectral applications of this approach, a significant challenge is presented by the low dimensionality of the spectral response (e.g., Landsat: seven channels, 8-bit data) relative to the high dimensionality of the typical forest landscape; hence, such multispectral classifications are often fundamentally and inherently "under-determined." The advantage of hyperspectral remote sensing is in the large number of narrow, contiguous spectral channels that better capture vegetation reflectance features than broadband sensors such as Landsat TM. Instead, one of the challenges presented by hyperspectral imaging spectroscopy is discerning from these high spectral dimension data the most meaningful spectral responses, i.e., those that help identify specific species (Underwood *et al.*, 2003; Williams and Hunt, 2002; Haskett and Sood, 1998).

Study Area and Field Data

The study site for this project was the Bartlett Experimental Forest (BEF) (44.06°N, 71.3°W) located within the White Mountain National Forest, a heavily forested and mountainous region in north central New Hampshire (Figure 1). Established in 1931 by the USDA Forest Service, Northeastern Research Station, the BEF is a 1,052 ha field laboratory for the study of secondary successional deciduous and coniferous forest dynamics and ecology. Major tree species represented include sugar maple (*Acer saccharum* L.), American beech (*Fagus grandifolia* Ehrn.), paper birch (*Betula papyrifera* Marsh.), yellow birch (*Betula alleghaniensis* Britt.), red maple (*Acer rubrum* L.), eastern hemlock (*Tsuga canadensis* L. Carr.), red spruce (*Picea rubens* Sarg.), and balsam fir (*Abies balsamea* (L.) Mill.), with localized small stands of eastern white pine (*Pinus strobus* L.). Most plots contain mixtures of two or more species. Species distributions reflect the interacting influences of climate, topography, forest management, and natural disturbance regimes.

Arrayed in a regular grid across the BEF are 441 intensively sampled 0.1 ha plots (see **http://www.fs.fed.us/ne/durham/4155/bartlett.htm**), which have been measured by 2.54 cm (1 inch) diameter classes in 1939 to 1940, 1991 to 1992, and 2001 to 2003. Plot elevations range from approximately 200 to 800 meters. Basal area and dry weight biomass (bole, branch, and foliar) were calculated by species for each inventory plot using regionally developed allometric equations based on stem diameter measurements (Jenkins *et al.*, 2004). Derived measures were stored in a geographic information system, referenced to New Hampshire State Plane coordinates (NAD83, GRS1980). Species composition as a fraction of total basal area was calculated for each plot from the most recent BEF survey data and used to help identify endmembers and perform accuracy assessment on the classifications (Figure 2).

Imagery

On 20 July 2001, NASA's Airborne Visible/Infrared Imaging Spectrometer (AVIRIS) was flown on the ER-2 platform (see

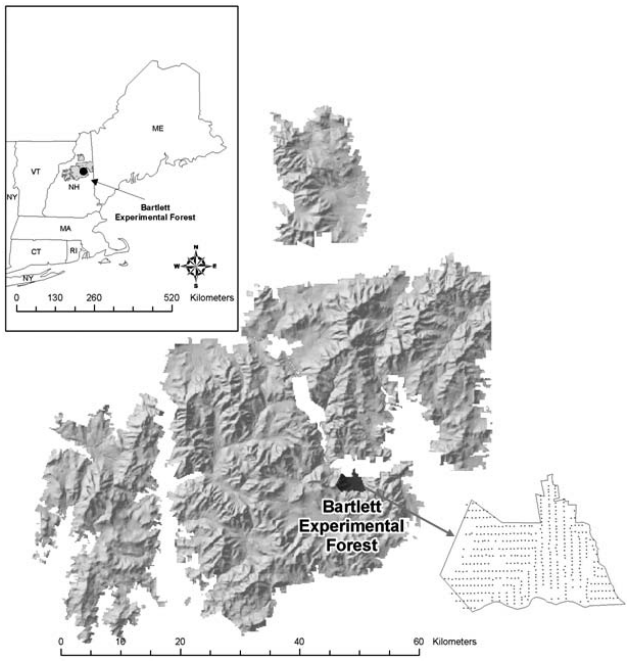

Figure 1. Location of the Bartlett Experimental Forest (BEF), Bartlett, New Hampshire, showing the established plot network.

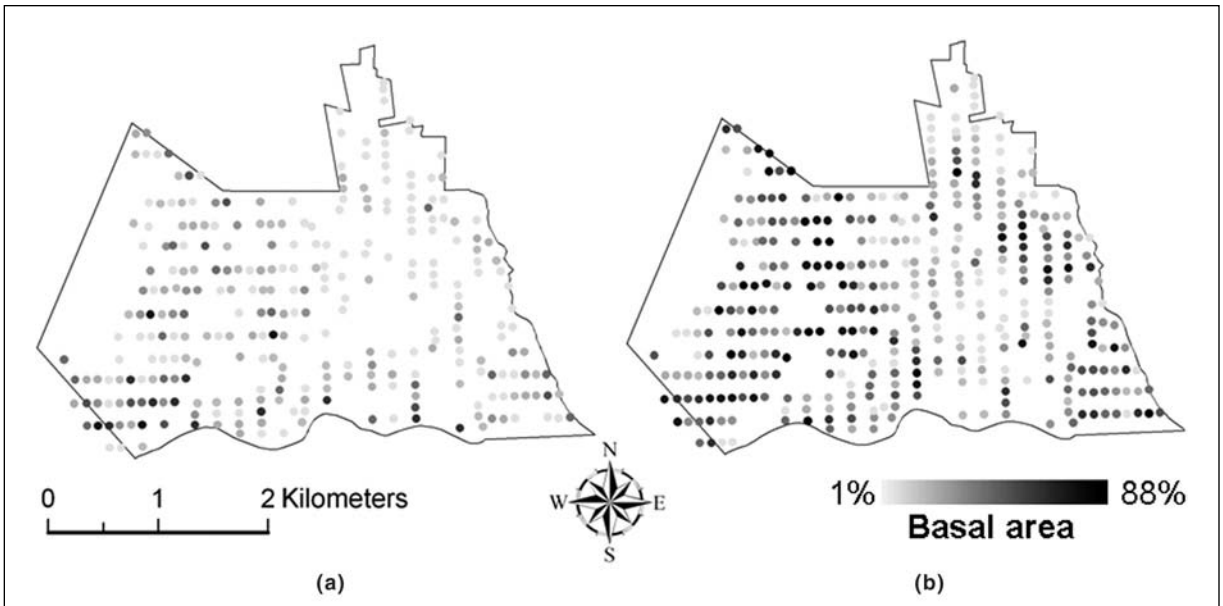

Figure 2. Fraction of sugar maple (a), and American beech (b) basal area measured at BEF.

http://aviris.jpl.nasa.gov/) and collected data in an 11 km by 20 km swath centered over the BEF, with approximately 10 percent cloud cover over the experimental forest. AVIRIS is a "whisk broom" scanner that captures upwelling spectral radiance in 224 contiguous spectral bands for wavelengths from 400 to 2,500 nm, with a 10 nm nominal bandwidth. The ER-2 flies at approximately 20 km above sea level, resulting in a pixel size of approximately 17 m. The AVIRIS images were delivered by NASA JPL as calibrated radiance data (*gain*μW/cm^2/nm/steradian*) and stored as 16-bit signed integers (IEEE) in BIP format.

On 29 August 2001, Hyperion collected data in a 7.5 km by 150 km swath centered over the BEF. Mounted on NASA's EO-1 satellite (see **http://eo1.gsfc.nasa.gov/Technology/Hyperion.html**), Hyperion orbits the earth at 705 km above sea level and one minute behind Landsat. Hyperion records radiance in the same spectral range as AVIRIS, with 10 nm spectral resolution, and 30 m spatial resolution. At the time of the overflight, conditions over BEF were cloud free. The data were delivered by USGS EROS Data Center as scaled radiance (*gain*W/m^2/μm/steradian*) (Level 1B1 correction) and stored in HDF format as signed 16-bit integers (IEEE) with BIL interleaving.

Preprocessing

Masks were generated for the AVIRIS and Hyperion images using the band range option in the ENVI (Version 3.6) software program (Research Systems, Inc., 2002) to remove clouds and non-vegetated areas (pavement and other developed surfaces, bare ground, water) in order to minimize under- or over-correction of vegetated areas when applying algorithms for normalization and atmospheric correction. In the AVIRIS image, masking clouds and cloud shadows left approximately 10 percent of the image unanalyzed. A "destreaking" program (Datt *et al.*, 2003; Jupp *et al.*, 2002) was applied to both Hyperion and AVIRIS images. While the destreaking process was originally developed to minimize a striping artifact present in Hyperion data (Jupp *et al.*, 2002), it also minimizes brightness gradients within AVIRIS scenes (Kennedy *et al.*, 1997) by normalizing the mean and standard deviation of each column of raster data to the overall mean and standard deviation of the image (e.g., Pontius *et al.*, 2005). Images were atmospherically corrected with ImSpec, LLC's Atmospheric Correction Now (ACORN®) (Version 4.14) software (**http://www.imspec.com**). Finally, each image was geo-registered with nearest neighbor resampling to 1992 USGS digital orthophotoquads (DOQ) with 1 m nominal spatial resolution acquired for the study area from the New Hampshire Geographically Referenced Analysis and Information Transfer System (NH GRANIT; **http://www.granit.sr.unh.edu**).

Image Classification

To assess the quality of the spectral channels (i.e., those with the most signal), each band was visually inspected using ENVI's animation and spectral profile tools, and bands whose signal was significantly diminished by atmospheric absorption of water, ozone, carbon dioxide, and other gases (Clark, 1999) were excluded from subsequent analyses. Excluding these wavelength regions, left 166 bands in the AVIRIS image and 152 bands in the Hyperion image for analyses (Table 1).

Both AVIRIS and Hyperion images were then transformed with a forward minimum noise fraction transform (MNF) rotation to segregate noise in the data as well as to reduce the computational requirements for subsequent SMA. While the MNF transformation was performed on all 166 AVIRIS bands, it was applied to only 61 Hyperion bands, excluding wavelength regions that were of particularly low signal-to-noise ratio (Smith *et al.*, 2003): <500 nm, 900 to 1,000 nm, 1,300 to 1,400 nm, and >2,000 nm. Twenty-five output MNF bands were selected based on the highest eigenvalues from the MNF rotation. A pixel purity index (PPI™; ENVI; Research Systems, Inc., 2002) was applied to the MNF images in order to find the most spectrally pure deciduous pixels. By iteratively projecting *n*-dimensional scatterplots onto a random unit vector, pixels that fall onto the ends of the unit vector are recorded and marked as "extreme" (Research Systems, Inc., 2002). Pixels that are repeatedly recorded as extreme correspond to the most pure spectra and are designated as endmembers. Endmember pixels identified in the PPI™ that correspond to deciduous forest-dominated pixels were saved as regions of interest (ROIs) and used to subset the 166-band AVIRIS and

TABLE 1. WAVELENGTHS RETAINED FOR IMAGE ANALYSIS

	AVIRIS		Hyperion	
	Number of Bands	Spectral Range (nm)	Number of Bands	Spectral Range (nm)
	6	451.37–499.72	6	**447.89–498.74**
	10	509.4–596.47	9	**508.91–590.26**
	10	606.15–692.72	10	600.43–691.96
	11	702.27–797.91	10	702.12–793.65
	10	807.49–893.83	10	803.82–895.34
	10	903.43–993.61	8	**905.51–993.25**
	11	1003.07–1097.65	2	**1003.37–1013.37**
	10	1107.11–1192.23	5	1154.65–1195.04
	11	1201.69–1293.37	10	1205.14–1295.92
	5	1303.34–1343.22	7	**1306.02–1366.51**
	5	1452.86–1492.72	6	**1447.2–1497.69**
	10	1502.69–1592.37	10	1507.79–1598.57
	10	1602.34–1692.01	10	1608.67–1699.45
	10	1701.97–1791.63	10	1709.55–1790.24
	6	2049.9–2099.93	11	**2002.1–2092.89**
	10	2109.93–2199.79	10	**2102.98–2193.77**
	10	2209.76–2299.38	10	**2203.87–2294.65**
	11	2309.33–2408.7	8	**2304.75–2365.24**
Total	166		152	

Note: Hyperion wavelengths in boldface type were excluded from the minimum noise fraction transform because of the relatively low signal-to-noise ratio in these channels.

61-band Hyperion data into deciduous forest images. A new forward MNF rotation was performed on these deciduous forest subsets, and pixels that corresponded to plots with the greatest percent basal area of sugar maple and beech were saved as endmember ROIs in both images.

Measured basal area never reached 100 percent for either sugar maple or American beech at BEF, so the next highest abundances were used as endmembers: 68 percent and 88 percent for sugar maple and beech, respectively. Six inventory plots were used to generate ROIs for sugar maple, and 12 inventory plots for beech. These ROI endmembers were then applied to ENVI's mixture-tuned matched filtering algorithm (MTMF™; Research Systems, Inc., 2002) to spatially estimate variation in sugar maple and American beech abundance in the AVIRIS and Hyperion MNF images. MTMF™, based on linear spectral unmixing (Boardman, 1994), is an SMA technique that maximizes the response of the known endmember in each pixel and suppresses the response of the remainder of the pixel (background), thus matching the known signature (endmember). This technique assigns each pixel a matched filter score, indicating how well the pixel matches the endmember used in the unmixing, where 1.00 is a perfect match, and values close to zero are background. It also produces an infeasibility score that can be used to eliminate false positives (Research Systems, Inc., 2002). Thus, the best results are pixels with relatively high-matched filter scores and relatively low infeasibility scores.

For a comparison of SMA results from hyperspectral data with those from broadband data, hardwood subset images from the 166-band AVIRIS and 152-band Hyperion were resampled to Landsat TM spectral bands with a Gaussian model using FWHM spacings (Research Systems, Inc., 2002). These resampled images were transformed with a forward MNF rotation, and the sugar maple and beech ROIs were each applied in an MTMF™ algorithm

Finally, for an additional comparison of SMA results with a broadly-classified forest cover type map, we used the BEF plot basal area data in a maximum likelihood classification of the 166-band AVIRIS dataset to identify sugar maple and beech. A sample of plots where sugar maple and beech comprised at least 60 percent of the basal area was used as training data in the maximum likelihood algorithm.

Accuracy Assessment

To assess the accuracy of the fractional abundance classifications derived from AVIRIS, Hyperion, and the simulated Landsat data, the results of the SMA were first scaled by 0.68 and 0.88 for sugar maple and American beech, respectively, in order to represent the maximum range in fraction of basal area as measured on the ground. For example, a perfect match between the sugar maple endmember (68 percent basal area) and an image pixel results in a matched filter value of 1.00; the scaled matched filter value in this case would be 0.68. Matched filter scores (excluding those that corresponded to infeasibility scores higher than 5, where infeasibility scores ranged from 1 to as high as 50) were then extracted from the AVIRIS and Hyperion SMA results and compared with basal area measurements from 150 plots in which sugar maple occurred and 200 plots in which beech occurred. Because the AVIRIS pixel size was 17 m and the field inventory plots were 30 m × 30 m (more than three times the area of a single AVIRIS pixel), SMA results from four pixels (34 m × 34 m) around each of the 150 and 200 plots were averaged in order to reduce error due to misalignment between an AVIRIS pixel and known plot coordinates. The spatial resolution of Hyperion (30 m), on the other hand, exactly matched the size of the field plots, so pixel aggregation was not necessary. Although some error due to misregistration is still possible in the Hyperion data, averaging values from four pixels would have introduced a larger additional source of error by inclusion of a substantially larger area than that represented by the reference plots. Once the SMA results were extracted, a simple linear regression was performed on the matched filter values against the fraction of basal area for these sample plots, and an R^2 and RMSE reported.

The accuracy of the maximum likelihood AVIRIS classification was assessed by creating an error matrix (Congalton and Green, 1999) in which field-measured data from sugar maple- and beech-dominated plots were compared to the results of the classification. The error matrix allowed for an estimate of overall accuracy, as well as evaluation of omission and commission errors (Congalton and Green, 1999). Omission errors represent the probability that a reference data pixel has not been correctly labeled in the classification; i.e., it has been *omitted* from the correct class. Commission errors represent the probability that a pixel from the classification is not labeled the same as the reference data pixel; i.e., it has been *committed* to another class. Also referred to as producer's and user's accuracies, respectively, omission and commission errors can often provide more information than one measure of accuracy.

Results

The SMA of sugar maple in AVIRIS and Hyperion resulted in similar spatial distributions of sugar maple (Figure 3a and 3b), but estimates of abundance varied between AVIRIS and Hyperion. AVIRIS results slightly underestimated sugar maple abundance, yet they were still more reliable than those derived from Hyperion, as evidenced in the higher R^2 and lower RMSE (Figure 4a and 4b; Table 2). Abundances estimated with both AVIRIS and Hyperion were more accurate at the lower end of the range (Figure 4a and 4b). When SMA was performed on AVIRIS and Hyperion data resampled to Landsat spectral bandwidths (Figure 3c and 3d), the relationship with measured sugar maple abundance deteriorated (Figure 4c and 4d; Table 2). Relative to the original AVIRIS data, the SMA of the Landsat bands simulated using AVIRIS resulted in a similar spatial pattern of sugar maple presence, but overestimated

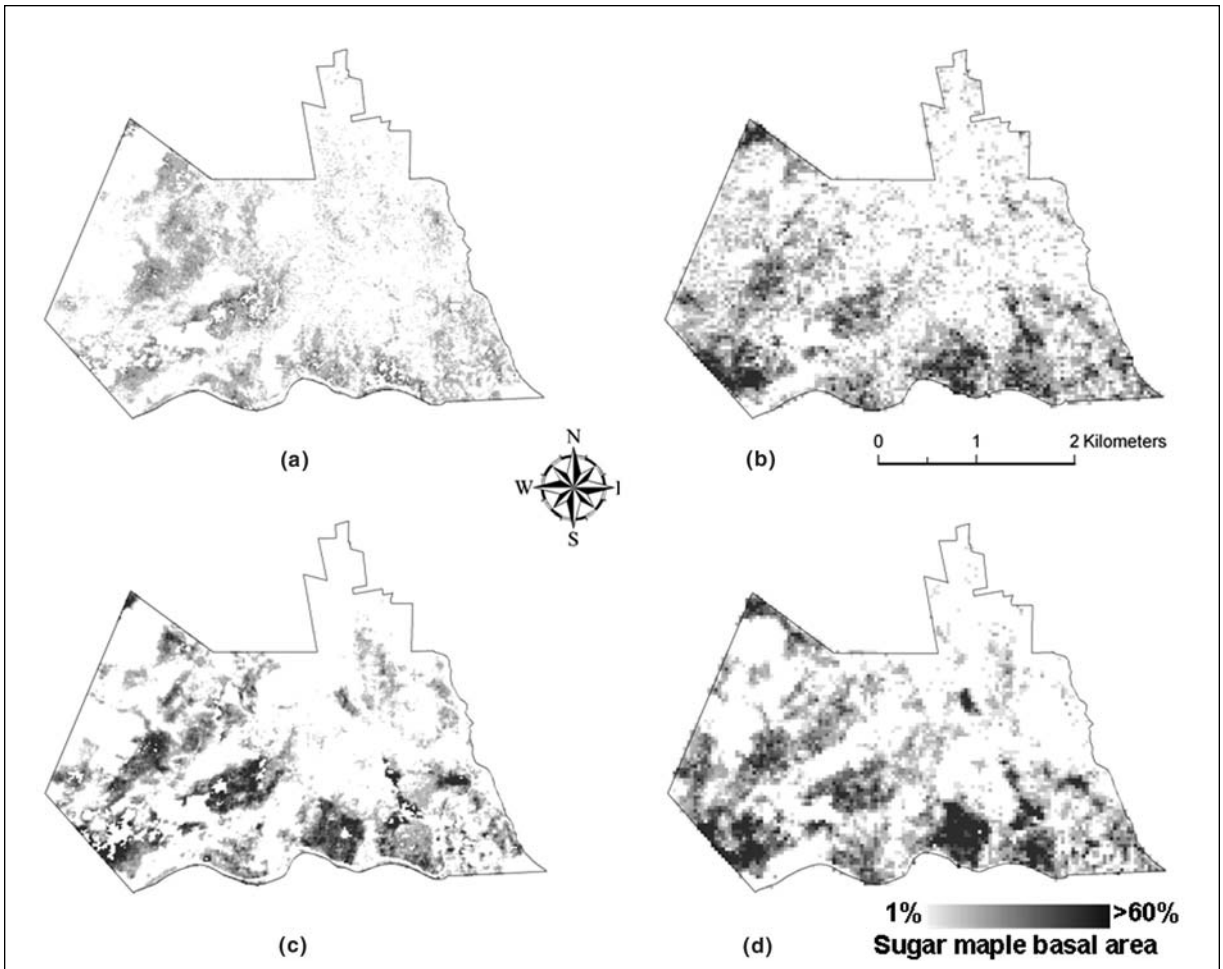

Figure 3. Sugar maple abundance maps generated from unmixing sugar maple pixels in AVIRIS (a) and Hyperion (b) imagery as well as AVIRIS and Hyperion imagery resampled to Landsat TM wavelengths (c and d, respectively). While both sensors detected similar spatial distribution patterns of sugar maple, Hyperion and the simulated Landsat TM data overestimated abundances of sugar maple.

abundance. The regression of sugar maple abundances derived from the AVIRIS-derived Landsat data indicated a poor overall relationship (Figure 4c), while the SMA of Hyperion data resampled to Landsat data resulted in still poorer results, with virtually no relationship (Figure 4d; Table 2).

Estimates of American beech abundance (Figure 5a through 5d) were less reliable overall than estimates of sugar maple, with higher RMSE from the regression (Table 2). While spectrally unmixing American beech from AVIRIS data resulted in slightly underestimated predictions of beech abundance, the SMA again produced better results for AVIRIS than for Hyperion (Figure 6a and 6b; Table 2). Results of American beech SMA on the data resampled to Landsat wavelengths (Figure 6c and 6d) were slightly lower than results from the original data, but not as poor as those from the sugar maple SMA, and similar to those from the original Hyperion data (Table 2).

The maximum likelihood classification (Figure 7) captured the overall spatial distribution of sugar maple and beech, together producing an overall accuracy of 70 percent (Table 3). Individual accuracies were better for beech than for sugar maple, with an estimated accuracy of 72 percent, an omission error of 28 percent, and a commission error of only 7 percent. Sugar maple, on the other hand, was classified with only 59 percent accuracy; with a commission error of 61 percent, more than half the classified sugar maple pixels were actually beech (Table 3).

Discussion

While moderate success was achieved overall with SMA of AVIRIS and Hyperion data, based on the regression analysis, we have more confidence in the results from AVIRIS than Hyperion (Table 2). When the data were resampled to the spectral coverage of Landsat, results were poor, especially for sugar maple. This suggests that broadband sensors such as Landsat do not have the level of spectral information necessary to resolve small-scale spectral features that help identify specific tree species such as sugar maple and beech. Herold *et al.* (2004) reported similar results in the ability of multispectral remote sensing to resolve specific spectral features in an urban environment. However, the moderate success of spectrally unmixing sugar maple and beech from AVIRIS, and to a lesser extent, Hyperion, demonstrates the potential of hyperspectral remote sensing for detecting species abundances, particularly for low abundance levels. Nevertheless, detecting species abundances in a heterogeneous forest is a complex problem, where a combination of factors contributes to errors.

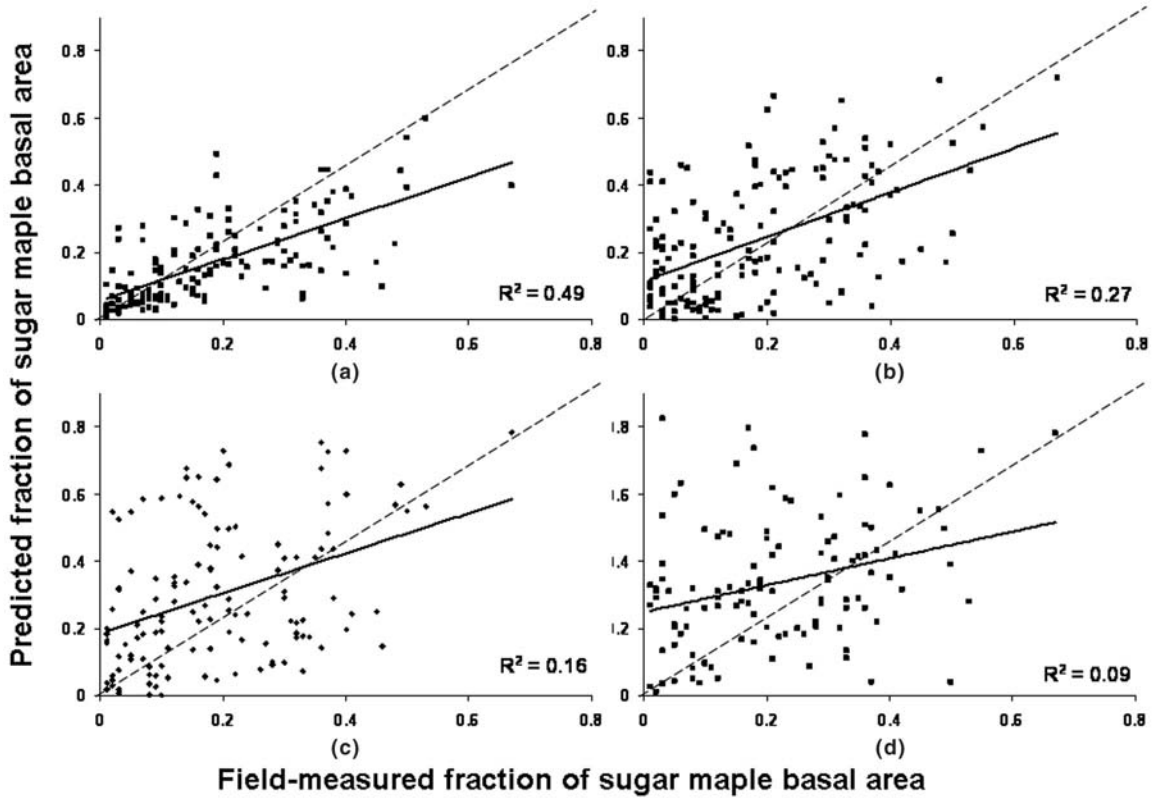

Figure 4. Linear regression of sugar maple abundances for 150 random samples. The dashed one-to-one line indicates that sugar maple abundance was slightly underestimated in the AVIRIS abundance map (a). The relationship between measured percent sugar maple basal area and that estimated from Hyperion (b), and Landsat data simulated with AVIRIS (c), and Hyperion (d) was not strong enough to make any meaningful generalizations.

TABLE 2. STATISTICS FROM LINEAR REGRESSION OF SMA RESULTS AGAINST MEASURED BASAL AREA FROM A SAMPLE OF PLOTS

	Sugar Maple (n = 150)					American Beech (n = 200)				
		SMA Results					SMA Results			
	Field Data	AV	AV Rsmpl	Hyp	Hyp Rsmpl	Field Data	AV	AV Rsmpl	Hyp	Hyp Rsmpl
mean	0.14	0.16	0.30	0.24	0.34	0.34	0.34	0.50	0.37	0.40
stdev	0.14	0.12	0.21	0.18	0.19	0.17	0.23	0.39	0.19	0.25
min	0.01	0.01	0.01	0.01	0.01	0.01	0.01	0.01	0.02	0.01
max	0.68	0.60	0.78	0.72	0.83	0.76	0.89	1.00	0.88	1.00
R^2		0.49	0.16	0.27	0.09		0.36	0.24	0.30	0.29
RMSE		0.09	0.19	0.15	0.18		0.18	0.33	0.16	0.21

AV: AVIRIS; AV Rsmpl: AVIRIS resampled to Landsat wavelengths; Hyp: Hyperion; Hyp Rsmpl: Hyperion resampled to Landsat wavelengths. All correlations were highly significant at the $p < 0.05$ level.

Sources of Error

Sources of error in estimating species abundances with SMA can be broadly attributable to one or more of the following components: (a) spectral similarities among species, (b) spatial overlap among species, (c) signal-to-noise ratio, (d) field measurement error, and (e) the accuracy assessment method.

The first component involves errors that result from species whose spectra are similar to one or more other species, and thus are prone to being confused with those other species. That is, when a species' spectral signature used as an endmember in SMA is similar to that of another species, the results of the classifications may be confounded. It is worth noting that we made an earlier attempt to identify spectrally pure endmembers of sugar maple and beech using a pixel purity index (PPI™; ENVI; Research Systems, Inc., 2002). While PPI™ worked well for discriminating deciduous- from conifer-dominated pixels (see the Methods section), it resulted in poor separability between species, so this method was abandoned for a manual selection of endmembers based on locations and abundances that were known from the BEF plot inventory data.

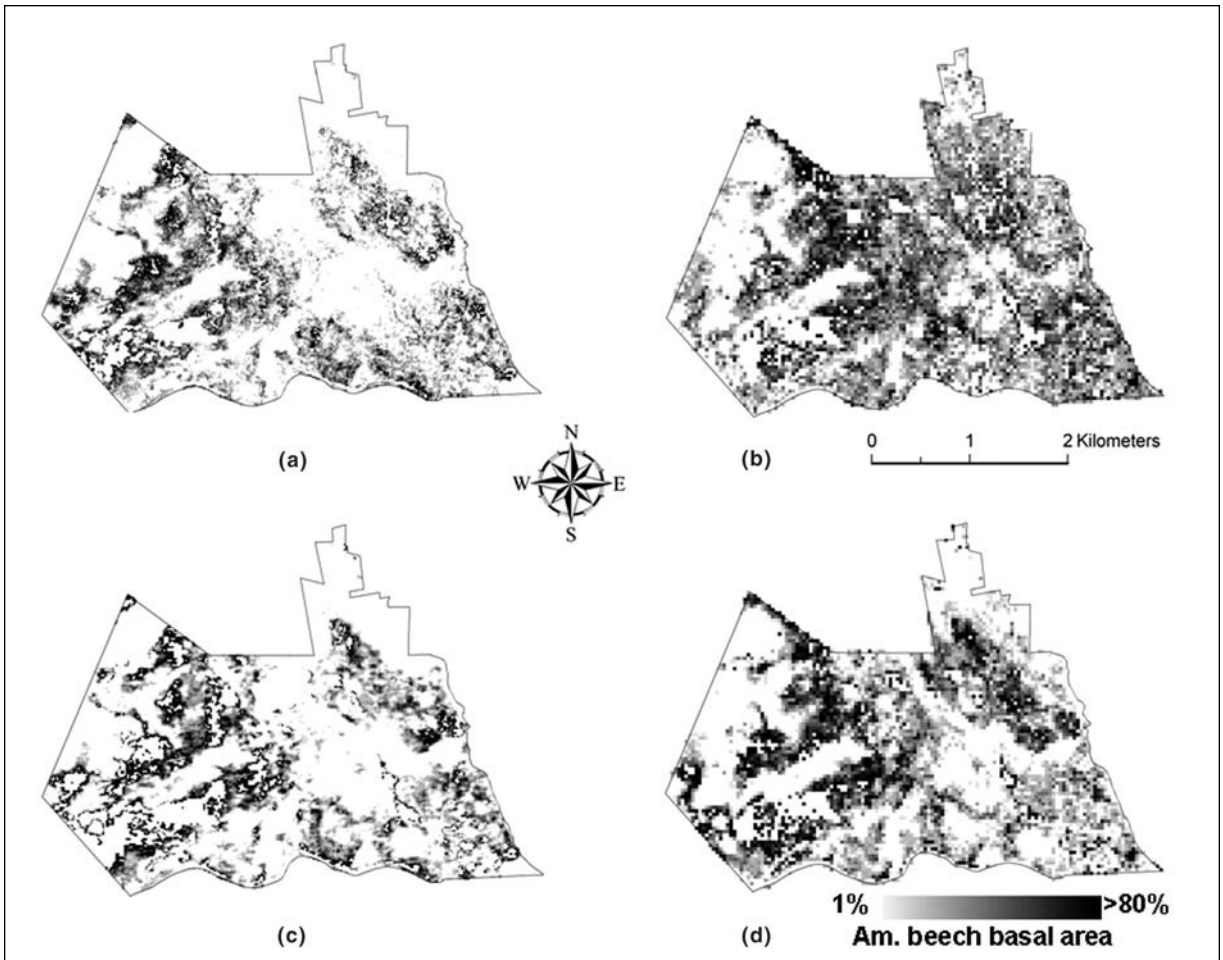

Figure 5. American beech abundance maps generated from unmixing beech pixels in AVIRIS (a), and Hyperion (b) imagery as well as AVIRIS and Hyperion imagery resampled to Landsat TM wavelengths (c and d, respectively). Similar to the results of the sugar maple unmixing, results from Hyperion and simulated Landsat data overestimated beech abundance.

Not surprisingly, classifying species that are spectrally unique in the image data typically results in a greater degree of separability. For example, Williams and Hunt (2002) had better success mapping leafy spurge in Wyoming with AVIRIS ($R^2 = 0.69$, $n = 66$) than we had mapping sugar maple and beech, but the authors noted that there were "no confounding groups with similar spectral signatures." Similarly, Underwood *et al.* (2003) achieved an overall accuracy of 75 percent when mapping non-native iceplant (*Carpobrotus edulis*) and jubata grass (*Cortaderia jubata*) on the California coast with AVIRIS. On the other hand, in a forest classification of the Central Appalachians using AVIRIS and Hyperion data, Foster and Townsend (2004) achieved lower than expected accuracies (65 percent and 60 percent for AVIRIS and Hyperion, respectively) for white oak (*Quercus alba*), the most abundant species in their study area. While this species is easily identified in the field, it often co-occurs with a number of functionally similar species, such as other *Quercus* species, and may be too spectrally similar to reliably separate in mixed pixels.

The second category of error is that resulting from the close spatial proximity of species relative to the pixel size of the instruments used to detect them. Individual pixels often include fine scale mixtures of species, and unless the image spatial resolution is fine enough to capture individual tree crowns, it remains challenging to classify tree species abundances in heterogeneous forests. At BEF, there are very few pure beech and sugar maple stands because these species co-occur nearly everywhere. For example, although sugar maple and beech were both present on 286 of 441 0.1 ha plots at BEF (Figure 8), sugar maple and/or beech co-occurred with other hardwoods (e.g., white ash, yellow birch, red maple) on 393 of 441 plots at BEF. All of our beech and sugar maple endmembers contained some background material that represented another hardwood, with the sugar maple endmembers containing the highest proportion. The problem of spatial overlap of species should be a greater factor in SMA results from Hyperion than from AVIRIS, given Hyperion's coarser pixel resolution and subsequently higher probability of capturing multiple species mixtures in individual pixels, and our results support this hypothesis.

A third source of error that likely affected our estimates of beech and sugar maple abundances is sensor signal-to-noise ratio (SNR). Together with spectral and spatial characteristics of species, data quality (reflected in SNR) affects endmember quality, which subsequently affects SMA results. While the northern hardwood species that characterize BEF are spectrally similar, imaging spectroscopy allows for some separation of these species, as evidenced in our relative success in estimating sugar maple abundance with AVIRIS. The fact that AVIRIS SMA results were better than

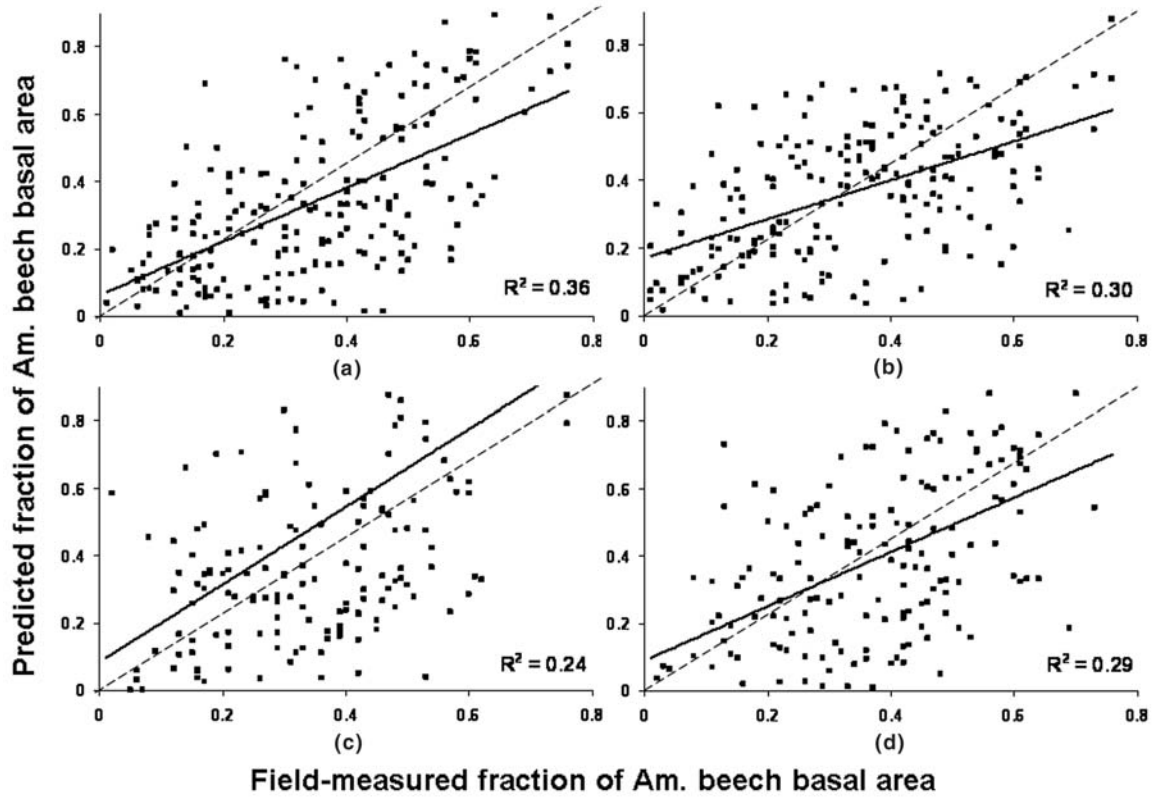

Figure 6. Linear regression of AVIRIS- and Hyperion-predicted American beech abundances for 200 random samples. The dashed one-to-one line and regression line indicate that beech abundances were slightly underestimated with AVIRIS (a), while there was only a weak relationship between beech abundances predicted with Hyperion (b), Landsat data simulated with AVIRIS (c) and Hyperion (d) and measured beech abundance.

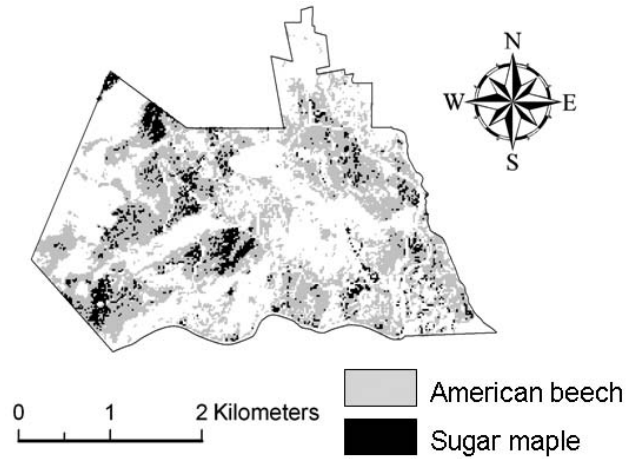

Figure 7. Results of maximum likelihood classification of AVIRIS data.

TABLE 3. CONTINGENCY TABLE OF MEASURED BASAL AREA VERSUS PIXELS LABELED AS BEECH AND SUGAR MAPLE IN A MAXIMUM LIKELIHOOD CLASSIFICATION OF THE AVIRIS DATASET

	Field Measurements			
Classification	Am. Beech	Sugar Maple	Row Total	Commission Error
American Beech	118	9	127	7%
Sugar Maple	27	17	44	61%
Not Classified	20	3	23	
Column Total	165	29	194	
Omission Error	28%	41%		
Estimated Classification Accuracy	72%	59%		
Overall Accuracy	(correctly classified pixels ÷ total pixels sampled) 70%			

Hyperion results, particularly for sugar maple, underscores the importance of data quality and suggests some role of SNR in our success with AVIRIS, given that AVIRIS SNR was nearly ten times higher than Hyperion SNR in 2001 (Kruse, 2003). Further, improvements to AVIRIS foreoptics in 2004 resulted in SNR nearly twice as high as in 2001 (Green, 2005). With these advances in data quality, we can likely expect stronger SMA results in future analyses.

The fourth potential source of error is field measurement data used for validation. According to Foster and Townsend (2004), forest inventory data may be only about

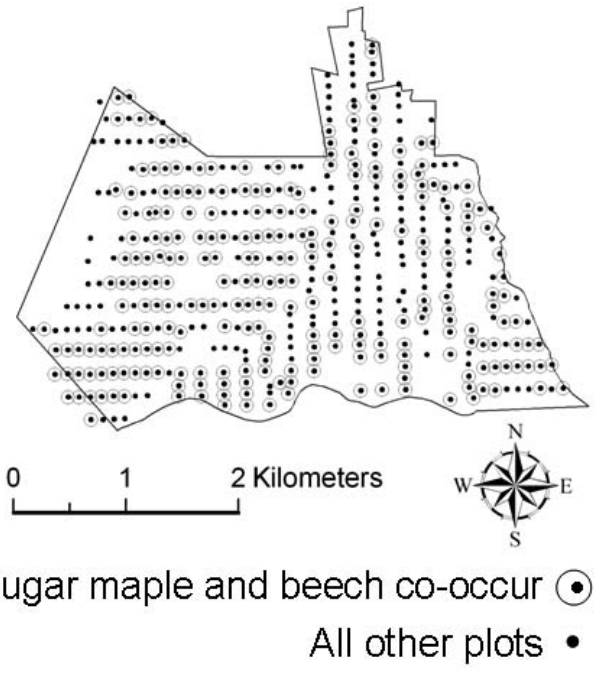

Figure 8. Spatial co-occurrence of sugar maple and beech within the grid of plots at BEF.

80 percent accurate, partly due to misidentified or misrecorded tree species. Further, within the field data, the specific variables used to evaluate the classifications can produce different apparent accuracies. For example, in this study basal area is an imperfect measure of species abundance in a forest canopy. Pontius *et al.* (2005) found that AVIRIS-predicted hemlock abundances in the Catskill region of New York State was often low with respect to field-measured basal area and attributed this to the inclusion of sub-canopy hemlock in basal area measurements that were not visible from above the canopy. This could also have affected results at BEF, where small-diameter beech and maple occur in the understory of many plots, and thus are included in plot percent basal area measurements. Because they are overtopped by canopy dominants and co-dominants, however, their spectral signatures may not impact the canopy spectral signature recorded by AVIRIS and Hyperion.

A final factor affecting the classification results is the method used for accuracy assessment. In other words, results from an error analysis may not be completely representative of the results of the classification. A simple linear regression of field-measured basal area against abundances estimated through SMA provides a measure of overall accuracy through an R^2 and RMSE, yet this may not explain all the variations in the classification. A contingency table or error matrix (Congalton and Green, 1999) can provide not only an overall measure of accuracy, but also the ability to quantify errors within specific ranges of abundances. Nevertheless, many classification and accuracy assessment techniques assume discrete land-cover classes, despite the fact that land-cover comprises an infinite variety of proportions and arrangements of water, soils, minerals, and woody and herbaceous biomass, so that it is nearly impossible to define all possible variations (Khorram, 1999). Even when classes are finely defined, class mixture and within-class variability will nearly always exist (Wang, 1990). Hence, fuzzy set theory, which makes use of a scale that defines *degrees* of error (Gopal and Woodcock, 1994; Congalton and Green, 1999), may prove useful for further interpretation of classification errors.

Finally, some degree of error in abundance estimates may reflect residual positional error rather than inaccuracy in the classification itself; while the AVIRIS and Hyperion images were registered to within approximately 4 meters overall of the DOQs, a digital elevation model was not used to remove the effects of topographic displacement. Given the large land area included in a Hyperion pixel (900 m^2), topographic displacement may have been more of an issue in the Hyperion imagery.

Underlying this discussion is the fact that using remote sensing to quantify the species abundance in heterogeneous forests is a challenging undertaking and requires consideration of a number of factors. However, many of the issues we have highlighted may be resolved in the future with relatively moderate effort. For example, while spectral similarities and spatial co-occurrence of species are problematic for selecting endmembers, this could be overcome with finer spatial resolution imagery, which is becoming increasingly available (e.g., data from the AVIRIS sensor mounted on low-flying aircraft such as a Twin Otter; see **http://aviris.jpl.nasa.gov/**). Smaller pixel size (e.g., on the order of 3 to 4 m pixels) would not only address the problems of spatial co-occurrence, but would also facilitate identification of pure endmembers. Better endmember selection is arguably the single most-important consideration in SMA. Part of Roberts *et al.* (1998) success in mapping California chaparral may have been due to the quality of field- and laboratory-measured reflectance spectra. In their work, field spectra were collected from a cherry picker using an Analytical Spectral Devices, Inc. full-range spectrometer, at heights ranging from 3 m to 5 m above the canopies. While topography and limited accessibility make this method infeasible for many areas within BEF, pure endmembers could be identified with higher resolution imagery, given the large crown size of mature northeastern trees. In addition, orthorectification should be performed on the imagery in order to include the effects of topography, particularly in an area such as the BEF, where elevation ranges from 200 to 900 m.

Spectral Mixture Analysis: Discrete Species Classes versus Species Abundance

In this analysis, use of SMA allowed us to derive an estimate of the fractional composition of sugar maple and beech for each pixel, even for small basal area fractions. Although our results contained prediction errors that stem from a number of factors, we view this approach as an important step forward from previously available methods. A conventional maximum likelihood classification classifies individual pixels only according to the dominant species or forest class, thereby omitting the potentially important contribution of other species present. For example, in a discrete classification that has 100 percent accuracy, a plot that is 40 percent sugar maple and 60 percent beech would be classified as beech, even though sugar maple plays an important functional role on that plot.

It is also important to note that validation statistics for discrete versus abundance-based forest type maps are not directly comparable, given that SMA produces continuous rather than categorical variables. For example, in a SMA approach, a pixel that has an actual sugar maple abundance of 65 percent that is predicted to be 80 percent sugar maple will contain an error of 15 percent, whereas a maximum likelihood approach using a 50 percent threshold would indicate no error. In a scenario where the predicted and observed sugar maple abundances are 30 percent and 45 percent, respectively, the same would hold true, despite the

fact that maximum likelihood omits sugar maple entirely. Indeed, plotting results from the discrete classification together with SMA results against field-measured basal area demonstrates how much information is lost with the more conventional approach (Figure 9). Hence, readers are cautioned not to take the higher apparent maximum likelihood accuracy values in Table 3 (72 percent and 59 percent for beech and sugar maple, respectively) as an indication of a more accurate characterization of the landscape than that generated by SMA. Despite the lower R^2 results from the SMA, the species abundance maps contain more information. The SMA is a more ambitious attempt at estimating species at BEF, and the lower R^2 values should be viewed in the context of the more challenging statistical test it reflects.

Conclusions and Future Work

The ability to detect fractional pixel composition (as opposed to classifying presence/absence of discrete forest types) stands to benefit a variety of ecological studies and should also be beneficial to spatial applications of ecosystem models. For example, Ollinger and Smith (2005) recently highlighted the need for this type of information in a spatial application of the PnET model (Aber *et al.*, 1995; Ollinger *et al.*, 1998) aimed at predicting landscape patterns of net primary production. Therefore, in light of the potential sources of error associated with species-level image classifications, the overall level of success achieved in this study suggests that while broadband multispectral data may not be suited to detailed species-specific analyses in heterogeneous forests in the northeast, application of SMA to hyperspectral data for species identification is a promising avenue of pursuit. Further, it is an approach that may be more appropriate than discrete classification in floristically diverse forests such as those in the northeastern U.S. region.

Future improvements may be realized through better SNR, finer spatial resolution, or fusion of hyperspectral data with other sensor data, such as lidar. Lidar remote sensing, in particular, offers promise in that it has been used to estimate basal area of Douglas fir and western hemlock in Oregon, in addition to biomass, leaf area index, and diameter at breast height (Lefsky *et al.*, 1999). As an ongoing extension to the research described here, work is underway to incorporate lidar metrics into the AVIRIS data cube to investigate whether this additional data layer can help better characterize stands, not only with respect to species, but also to age, disturbance, and land-use history.

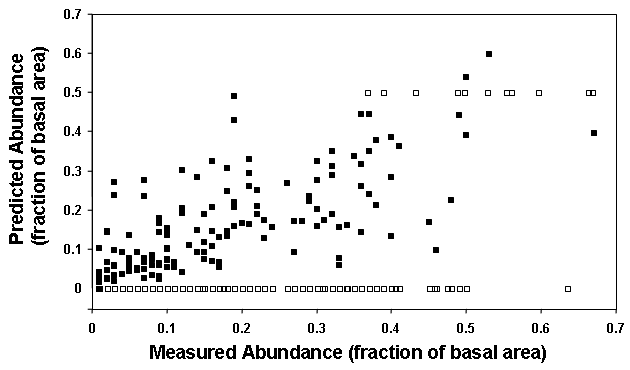

Figure 9. Sugar maple abundance (fraction of stand basal area) as estimated with spectral mixture analysis (solid squares) and maximum likelihood classification (open squares) plotted against field-measured values. Because the maximum likelihood method is designed only to detect sugar maple presence or absence relative to a prescribed threshold, abundance can only be estimated as one of two fixed values, in this case 0 and 50 percent, based on the threshold used in this study. (Some plots are not shown for both methods because plots used either as training areas or endmembers were not included.) This comparison is shown to illustrate the difference between approaches in terms of how much information each attempts to capture. Similarly, because accuracy assessment methods are typically designed relative to what a particular approach attempts to accomplish, a maximum likelihood classification may prove to be 100 percent accurate despite the lesser amount of information it contains.

Acknowledgments

This research was supported by the NASA Carbon Cycle Sciences Program (Grants CARBON/0000-0243 and CARBON/04-0120-0011), the NASA EO-1 validation program (Grant NCC5-477), and the U.S. Department of Energy's National Institute of Global Environmental Change (NIGEC Grant UNH901214-02). Portions of this research were based upon data generated in long-term research studies on the Bartlett Experimental Forest, funded by the U.S. Department of Agriculture, Forest Service, Northern Research Station. Acquisition of AVIRIS imagery was made possible by generous support from the Jet Propulsion Laboratory's AVIRIS Science and Instrument Teams and the NASA Terrestrial Ecology Program.

References

Aber, J.D., S.V. Ollinger, C.A. Federer, P.B. Reich, M.L. Goulden, D.W. Kicklighter, J.M. Melillo, and R.G. Lathrop, Jr., 1995. Predicting the effects of climate change on water yield and forest production in the northeastern United States, *Climate Research*, 5:207–222.

Alberotanza, L., V.E. Brando, G. Ravagnan, and A. Zandonella, 1999. Hyperspectral aerial images: A valuable tool for submerged vegetation recognition in the Orbetello Lagoons, Italy, *International Journal of Remote Sensing*, 20(3):523–533.

Allison, S.D., and P.M. Vitousek. 2004. Rapid nutrient cycling in leaf litter from invasive plants in Hawaii, *Oecologia*, 141 (4):612–619.

Asner, G.P., C.E. Borghi, and R.A. Ojeda, 2003. Desertification in central Argentina: Changes in ecosystem carbon and nitrogen from imaging spectroscopy, *Ecological Applications*, 13(3): 629–648.

Bailey, S.W., S.B. Horsley, R.P. Long and R.A. Hallett, 2004. Influence of edaphic factors on sugar maple nutrition and health on the Allegheny Plateau, *Soil Science Society of America Journal*, 68:243–252.

Boardman, J.W., 1994. Geometric mixture analysis of imaging spectrometry data, *Proceedings of the Geoscience and Remote Sensing Symposium, IGARSS '94, Surface and Atmospheric Remote Sensing: Technologies, Data Analysis and Interpretation*, 08–12 August, Pasadena, California, Volume 4, pp. 2369–2371.

Chokkalingam, U., and A. White, 2001. Structure and spatial patterns of trees in old-growth northern hardwood and mixed forests of northern Maine, *Plant Ecology*, 156(2):139–160.

Clark, R.N., 1999. Spectroscopy of rocks and minerals, and principles of spectroscopy, *Manual of Remote Sensing, Volume 3, Remote Sensing for the Earth Sciences* (A.N. Rencz, editor), John Wiley and Sons, New York, pp. 3–58.

Congalton, R.G., and K. Green, 1999. *Assessing the Accuracy of Remotely Sensed Data: Principles and Practices*, Lewis Publishers, New York, 137 pp.

Datt, B., T.R. McVicar, T.G., Van Niel, D.L.B. Jupp, and J.S. Pearlman, 2003. Preprocessing EO-1 Hyperion hyperspectral data to support the application of agricultural indexes, *IEEE Transactions on Geoscience and Remote Sensing*, 41(2):1246–1259.

Dennison, P.E., and D.A. Roberts, 2003. Endmember selection for multiple endmember spectral mixture analysis using endmember average RMSE, *Remote Sensing of Environment*, 87:123–135.

Drohan, P.J., S.L. Stout, and G.W. Petersen, 2002. Sugar maple (*Acer saccharum* Marsh.) decline during 1979–1989 in northern Pennsylvania, *Forest Ecology and Management*, 170(1–3):1–17.

Elmore, A.J., J.F. Mustard, S.J. Manning, and D.B Lobell, 2000. Quantifying vegetation change in semiarid environments: Precision and accuracy of spectral mixture analysis and the normalized difference vegetation index, *Remote Sensing of Environment*, 73:87–102.

Finzi, A.C., N. Van Breemen, and C.C. Canham, 1998. Canopy tree-soil interactions within temperate forests: Species effects on soil carbon and nitrogen, *Ecological Applications*, 8:440–446.

Foster, J.R., and P.A. Townsend, 2004. Linking hyperspectral imagery and forest inventories for forest assessment in the central Appalachians, *Proceedings of the 14th Central Hardwood Forest Conference*, 16–19 March, Wooster, Ohio, U.S. Department of Agriculture, Forest Service, Northeastern Research Station General Technical Report NE-316, Newtown Square, Pennsylvania, pp. 76–86.

Gansner, D.A., S.L. King, S.L. Arner, and D.A. Drake, 1996. Mapping shifts in the relative stocking of tree species, *Northern Journal of Applied Forestry*, 13(2):92–95.

García-Haro, F.J., M.A. Gilabert, and J. Meliá, 1996. Linear spectral mixture modeling to estimate vegetation amount from optical spectral data, *International Journal of Remote Sensing*, 17(17): 3373–3400.

Gilabert, M.A., F.J. García-Haro, and J. Meliá, 2000. A mixture modeling approach to estimate vegetation parameters for heterogeneous canopies in remote sensing, *Remote Sensing of Environment*, 72:328–345.

Gong, P., J.R. Miller, and M. Spanner, 1994. Forest canopy closure from classification and spectral unmixing of scene components-multisensor evaluation of an open canopy, *IEEE Transactions on Geoscience and Remote Sensing*, 32(5):1067–1080.

Gong, P., R. Pu, and B. Yu, 1997. Conifer species recognition: An exploratory analysis of *in situ* hyperspectral data, *Remote Sensing of Environment*, 62:189–200.

Gopal, S., and C. Woodcock, 1994. Theory and methods of accuracy assessment using fuzzy sets, *Photogrammetric Engineering & Remote Sensing*, 60(2):181–188.

Green, R.O., 2005. The AVIRIS radiometric performance model and current signal-to-noise-ratio performance, *Proceedings of the 14th JPL Airborne Geoscience Workshop*, Jet Propulsion Laboratory, 25–27 May, Pasadena, California (in press).

Hane, E.N. 2003. Indirect effects of beech bark disease on sugar maple seedling survival, *Canadian Journal of Forest Research*, 33(5):807–813.

Haskett, H.T., and A.K. Sood, 1998. Trade-off studies of detection performance versus the number of reflective spectral bands in hyperspectral imagery, *Proceedings of the SPIE Conference on Algorithms for Multispectral and Hyperspectral Imagery IV*, April, Orlando, Florida, SPIE, Vol. 3372, pp. 26–42.

Herold, M., D.A. Roberts, M.E. Gardner, P.E. Dennison, 2004. Spectrometry for urban area remote sensing-Development analysis of a spectral library from 350 to 2400 nm, *Remote Sensing of Environment*, 91:304–319.

Horsley, S.B., R.P. Long, S.W. Bailey, R.A. Hallett, and T. Hall, 2000. Factors associated with decline disease of sugar maple on the Allegheny Plateau. *Canadian Journal of Forest Research*, 30:1365–1378.

Houston, D.R., 1994. Major new tree disease epidemics: Beech bark disease, *Annual Review of Phytopathology*, 32:75–87.

Iverson, L.R., M.E. Dale, C.T. Scott, and A. Prasad, 1997. A GIS-derived integrated moisture index to predict forest composition and productivity of Ohio forests (USA), *Landscape Ecology*, 12(5):331–348.

Jenkins, J.C., D.C. Chojnacky, L.S. Heath, R.A. Birdsey, 2004. *Comprehensive Database of Diameter-based Biomass Regressions for North American Tree Species*, General Technical Report NE-319, Newtown Square, Pennsylvania, U.S. Department of Agriculture, Forest Service, Northeastern Research Station, 45 p., on CD-ROM.

Jupp, D.P.L., B. Datt, J. Lovell, and E. King, 2002. *EO-1/Hyperion Data Workshop Notes*, April, Canberra, Australia, CSIRO Office of Space Science and Applications, Earth Observation Centre.

Kennedy, R.E., W.B. Cohen, and G. Takao, 1997. Empirical methods to compensate for a view-angle-dependent brightness gradient in AVIRIS imagery, *Remote Sensing of Environment*, 62:277–291.

Khorram, S., G.S. Biging, N.R. Chrisman, D.R. Colby, R.G. Congalton, J.E. Dobson, R.L. Ferguson, M.F. Goodchild, J.R. Jensen, and T.H. Mace, 1999. *Accuracy Assessment of Remote Sensing-derived Change Detection*, Monograph, American Society for Photogrammetry and Remote Sensing, Bethesda, Maryland, 64 p.

Kokaly, R.F., D.G. Despain, R.N. Clark, and K.E. Livo, 2003. Mapping vegetation in Yellowstone National Park using spectral feature analysis of AVIRIS data, *Remote Sensing of Environment*, 84:437–456.

Kruse, F.A., 2003. Mineral mapping with AVIRIS and EO-1 Hyperion, *Proceedings of the 12th JPL Airborne Geoscience Workshop*, 25–28 February, Pasadena, California, Jet Propulsion Laboratory Publication 04–6, pp.149–156, on CD-ROM.

Leak, W.B., 1982. *Habitat Mapping and Interpretation in New England*, U.S. Department of Agriculture Forest Service Research Paper NE-496.

Leckie, D.G., F.A. Gougeon, N. Walsworth, and D. Paradine, 2003. Stand delineation and composition estimation using semi-automated individual tree crown analysis, *Remote Sensing of Environment*, 85(3):355–369.

Lefsky, M.A., W.B. Cohen, S.A. Acker, G.G. Parker, T.A. Spies, and D. Harding, 1999. Lidar remote sensing of the canopy structure and biophysical properties of Douglas-fir western hemlock forests, *Remote Sensing of Environment*, 70:339–361.

Lovett, G.M., and H. Rueth, 1999. Soil nitrogen transformations in beech and maple stands along a nitrogen deposition gradient, *Ecological Applications*, 9:1330–1344.

Lovett, G.M., K.C. Weathers, M.A. Arthur, and J.C. Schultz, 2004. Nitrogen cycling in a northern hardwood forest: Do species matter?, *Biogeochemistry*, 67(3):289–308.

Martin, M.E., S.D. Newman, J.D. Aber, and R.G. Congalton, 1998. Determining forest species composition using high spectral resolution remote sensing data, *Remote Sensing of Environment*, 65:249–254.

Ollinger, S.V., J.D. Aber, and C.A. Federer, 1998. Estimating regional forest productivity and water yield using an ecosystem model linked to a GIS, *Landscape Ecology*, 13:323–334.

Ollinger, S.V., and M.-L. Smith, 2005. Net primary production and canopy nitrogen in a temperate forest landscape: An analysis using imaging spectroscopy, modeling, and field data, *Ecosystems*, 8:1–19.

Pontius, J., R. Hallett, M. Martin, 2005. Using AVIRIS to assess hemlock abundance and early decline in the Catskills, NY, *Remote Sensing of Environment*, 97(2):163–173.

Puttock, G.D., I. Timossi, and L.S. Davis, 1998. BOREAL: A tactical planning system for forest ecosystem management, *Forestry Chronicle*, 74(3):413–420.

Radeloff, V.C., D.J. Mladenoff, and M.S. Boyce, 1999. Detecting jack pine budworm defoliation using spectral mixture analysis: Separating effects from determinants, *Remote Sensing of Environment*, 69:156–169.

Research Systems, Inc., 2002. *ENVI User's Guide*, Version 3.6.

Roberts, D.A., M. Gardner, R. Church, S. Ustin, G. Scheer, and R.O. Green, 1998. Mapping chaparral in the Santa Monica mountains using multiple endmember spectral mixture models, *Remote Sensing of Environment*, 65:267–279.

Sandmeier, S., and D.W. Deering, 1999. Structure analysis and classification of boreal forests using airborne hyperspectral

BRDF data from ASAS, *Remote Sensing of Environment*, 69:281–295.

Schriever, J.R., and R.G. Congalton, 1995. Evaluating seasonal variability as an aid to cover-type mapping from Landsat Thematic Mapper data in the Northeast, *Photogrammetric Engineering & Remote Sensing*, 61(3):321–327.

Smith, M.L., M.E. Martin, S.V. Ollinger, and L. Plourde, 2003. Analysis of hyperspectral data for estimation of temperate forest canopy nitrogen concentration: Comparison between an airborne (AVIRIS) and a spaceborne (Hyperion) sensor, *IEEE Transactions on Geosciences and Remote Sensing*, 41(6): 1332–1337.

Sohn, Y., and R.M. McCoy, 1997. Mapping desert shrub rangeland using spectral unmixing and modeling spectral mixtures with TM data, *Photogrammetric Engineering & Remote Sensing*, 63(6):707–716.

Spetich, M.A., G.R. Parker, and E.J. Gustafson, 1997. Spatial and temporal relationships of old-growth and secondary forests in Indiana, USA, *Natural Areas Journal*, 17(2):118–130.

Underwood, E., S. Ustin, and D. DiPietro, 2003. Mapping nonnative plants using hyperspectral imagery, *Remote Sensing of Environment*, 86:150–161.

Ustin, S.L., and Q.F. Xiao, 2001. Mapping successional boreal forests in interior central Alaska, *International Journal of Remote Sensing*, 22(6):1779–1797.

Wang, F., 1990. Improving remote sensing image analysis through fuzzy information representation, *Photogrammetric Engineering & Remote Sensing*, 56(8):1163–1169.

Watson, N., and D. Wilcock, 2001. Preclassification as an aid to the improvement of thematic and spatial accuracy in land cover maps derived from satellite imagery, *Remote Sensing of Environment*, 75:267–278.

Williams, A.P., and E.R. Hunt, Jr., 2002. Estimation of leafy spurge cover from hyperspectral imagery using mixture tuned matched filtering, *Remote Sensing of Environment*, 83:446–456.

Woodcock, C.E., J.B. Collins, S. Gopal, V.D. Jakabhazy, X. Li, S., Macomber, S. Ryherd, V.J. Harward, J. Levitan, and Y. Wu, 1994. Mapping forest vegetation using Landsat TM imagery and a canopy reflectance model, *Remote Sensing of Environment*, 50(3):240–254.

(Received 18 October 2005; accepted 08 December 2005; revised 31 January 2006)